Research Article

Waveform Characteristics of Tunnel Blast Waves and a Wave-Blocking Method

Xianshun Zhou [ID],[1,2] **Xuemin Zhang** [ID],[1,2] **Tianhe Ren,**[3] **Xuefeng Ou** [ID],[4] **Wenchao Xiong,**[1,2] **Liming Zhang,**[3] **and Lei Zhang**[3]

[1]*School of Civil Engineering, Central South University, Changsha, Hunan 410075, China*
[2]*Key Laboratory of Heavy-haul Railway Engineering Structure, Ministry of Education, Central South University, Changsha, Hunan 410075, China*
[3]*Guizhou Highway Engineering Group Co., Ltd., Guiyang 550000, China*
[4]*School of Civil Engineering, Changsha University of Science & Technology, Changsha, Hunan 410114, China*

Correspondence should be addressed to Xuemin Zhang; zhangxm@csu.edu.cn

The impact of blast wave air overpressure (AOp) may cause damage to nearby structures and significant noise pollution. In order to minimize the impact of the blast wave on the buildings around the tunnel, a new wave-blocking trolley (NWBT) was proposed to control the AOp during the construction of the Baitacun tunnel, as the nearby villages were located less than 100 m from the tunnel portal. In the study, the characteristics of the blast wave pressure profiles were studied by field measurements and numerical simulations and the Friedlander equation parameters were obtained. Second, the controlling effect and working mechanism of the NWBT were verified to be effective. The measured peak AOp was weakened from 2.49 kPa to 0.55 kPa with the operating NWBT, which meets the requirements of Chinese specifications. Furthermore, a numerical simulation for the impact process of the NWBT was established using the ANSYS/LS-DYNA software. Finally, it was found that a shorter distance from the NWBT to the source of the blast makes a better contribution to its wave-blocking effect. The waveform characteristics obtained in the study contribute to the design of tunnel surrounding structures; the application of the NWBT is a successful wave-blocking method for tunnels adjacent to environmentally sensitive areas.

1. Introduction

In blast work, a considerable portion of explosive energy is wasted in the form of undesirable environmental side effects, such as ground vibrations and air blasts [1]. When blasting work is repeatedly performed in neighboring towns, the ground peak particle velocity and air overpressure (AOp) create significant annoyance to personnel and residents [2], and it can even cause the breakage of glass, loss of a decorative layer, and displacement of doors and windows [3, 4].

Fang [5] and Rodríguez [6, 7] have obtained the blast waves propagation characteristics in tunnel generated by rock fragmentation works, but these literatures only focused on the peak of AOp. When the destructive effects of blast waves need to be studied, the waveforms first need to be analyzed and mathematically described. In a typical free-field explosion, the blast waves decay in a spherical wave radially in all directions. The waveform of the blast wave exhibits nonlinear decay behind the shock front, and its simplified overpressure-time curve can be described mathematically by the Friedlander equation [8]. The equation cannot be used to describe the near field, but it is well adapted for the far field [9]. The most widely used Friedlander equations have been studied experimentally for spherical explosions and incident blast waves. For this case, the explosion was assumed to have occurred mid-air, and the resulting blast wave spherically propagated outward [10]. However, there are few descriptions for blast wave induced

by tunnelling rock fragmentation. In contrast to blast waves that radiate in all directions, a wave in a finite space undergoes planar propagation in one direction toward the opening, and the pressure profiles can be very different [11].

In addition, when the blasting operation is close to residential buildings, some preconstructed devices to reduce blast AOp are necessary [12]. The air door with a magnetic lock was used to protect against gas explosion in a coal mine [13], but the device is complex and not suitable for large cross-sectional traffic tunnel. A temporary but inconvenient wave-blocking door was commonly placed at the tunnel portal, which was made of bamboo and rubber [14]. And also, the blast wave attenuation can be accelerated by the spoilers in the tunnel [15, 16]. The spoilers are a series of flat plates installed on the tunnel wall at a certain distance apart, working at an angle with the direction of the blast wavefront. Although these devices are not entirely suitable for tunnel constructions, it can be known from these applications that when the air blast wave propagates in one direction from the blasting face to the tunnel portal, the AOp could be weakened significantly if a flexible buffer device was established on the propagation path.

Nowadays, ANSYS/LS-DYNA is used widely to simulate dynamic processes and to solve the continuum equations for nonlinear responses of materials and structures. The software was successfully used in the dynamics analysis such as spoiler wave attenuation [15], aircraft bird striking [17], bulletproof materials [18], and rockfall [19]. Therefore, numerical simulations can be used to analyze the action process of wave-blocking.

The innovations and main contributions of the paper are described as follows:

First, the field experiments were conducted to obtain the shapes and magnitudes of blast waveforms, especially the pressure profiles, during tunnel blasting engineering.

Then, a new wave-blocking trolley (NWBT) was proposed to control the blast AOp. The device was applied in the Baitacun tunnel in Yunnan, China, and the wave-blocking effect of the AOp was tested.

Furthermore, a numerical model was established using the ANSYS/LS-DYNA software to analyze the propagation characteristics during the wave-blocking process; and the optimal working area of NWBT in the tunnel was studied.

2. Theoretical of Friedlander Equation

In a typical Friedlander waveform (Figure 1), the ambient pressure P_a is a reference for the positive and negative pressure values. After an explosion, the blast wave reaches a target point in time t_0, and with time, it reaches the peak AOp P^*. The trend continues in the negative direction. After reaching the negative pressure, the pressure then gradually oscillates back to the ambient pressure P_a. The previous research has focused on the positive phase of the blast wave characteristics, which in most cases is more critical to the structural safety.

According to the Friedlander equation, the overpressure $P(t)$ depends on time t, which is measured after the arrival of the shock front to the point of interest, as follows:
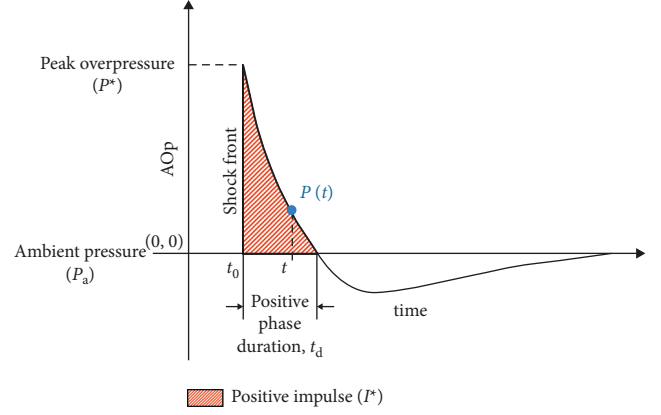

FIGURE 1: Typical Friedlander waveform.

$$P(t) = P * \left(1 - \frac{t - t_0}{t_d} \right) e^{-bt - t_0/t_d}, \tag{1}$$

where P^* is the peak overpressure, t_0 is the arrival time of the shock front, t_d is the positive phase duration, and b is a decay coefficient of the waveform.

The blast wave is also characterized by a positive impulse I^*, which is related to the total pressure volume applied on a structure due to an explosion, calculated through the integration of the pressure-time curve as follows:

$$I^* = \int_{t_0}^{t} P(t) \mathrm{d}t = P * t_d \left[\frac{1}{b} - \frac{1 - e^{-b}}{b^2} \right]. \tag{2}$$

From this equation, the most relevant factors for I^* are the peak pressure P^* and the positive duration t_d, which also have a high correlation with the coefficient b.

3. Full-Scale Experiments

3.1. Engineering Background. The Baitacun tunnel is located on the Dali-Nanjian Expressway, Yunnan Province. It is a double-hole tunnel, with a length of 10.79 km. The densely populated residential buildings are within 100 m of the tunnel portal which are susceptible to blasting AOp. Figure 2 shows the site environment near the tunnel portal. The closest distance to the tunnel portal is only 61.2 m.

3.2. Blasting Experiment Scheme. The dimensions of the tunnel cross section were 12.78 m × 10.78 m (width × height), with a horseshoe shape. In order to control the total weight of the explosive, a section was broken at several areas, and millisecond delayed blasting was used. The blasting holes and parameters are shown in Figure 3. The diameter of the blasting hole was 42 mm. The cutting holes and collapsing holes were tilted, and the other holes were perpendicular to the blast face. The depths of the cutting holes were 2.8 m, with a drilling angle of 70°. The depths of the collapsing holes were 2.9 m, and their angles were 80°. The depths of other holes were 2.2 m. The blast is induced by an emulsion explosive, which has high water resistance, and nonelectric millisecond delay detonators. The total weight of
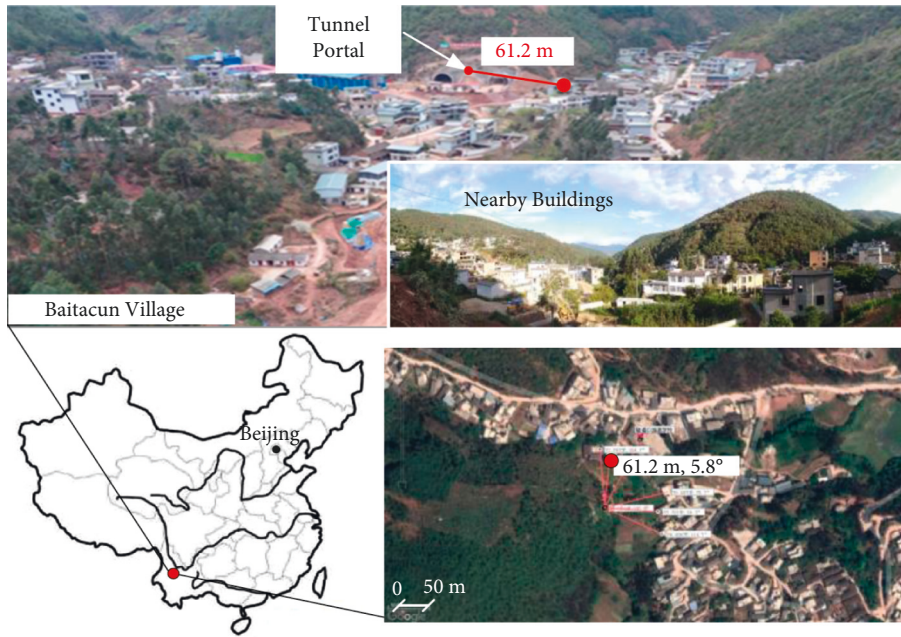
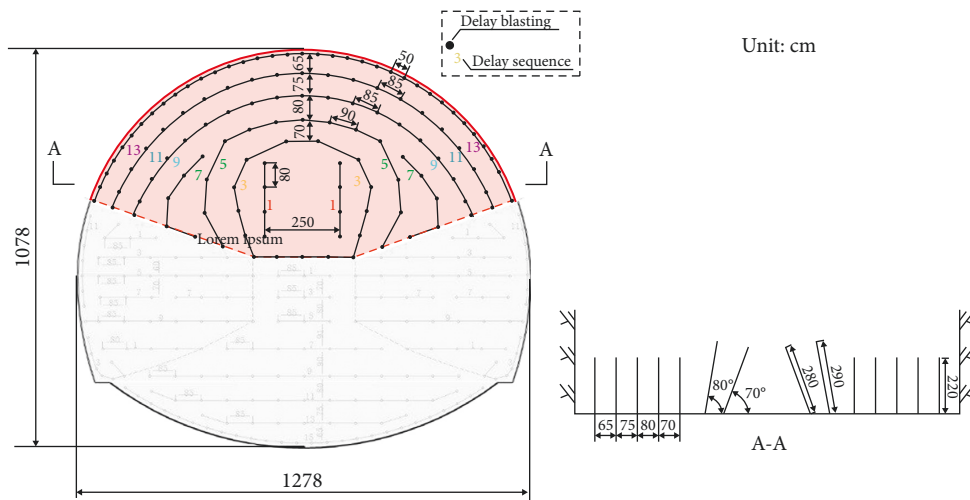Figure 2: Overview of the area near the tunnel portal.

Figure 3: Blasting experiment scheme.

explosives Q was approximately 96.0 kg, and the maximum weight q_{max} of all the sequences was 7.6 kg.

3.3. Design of NWBT.

As the residential buildings are susceptible to AOp from tunnel blast, a preconstructed trolley for wave-blocking is designed. Figure 4 depicts the details of the NWBT. It consisted of a framework gantry, louvered acoustic panels, wave-blocking curtains, and other ventilation and moving accessories. The outer edge of the NWBT matched the inner profile of the tunnel lining; and the structural material of NWBT was I-beam. The door curtain was closed during blasting and was usually opened to avoid disrupting traffic.

The installation sequence of the NWBT is shown in Figure 5. The NWBT was assembled outside the tunnel. The framework gantry consisted not only of columns and beams but also of the necessary diagonal braces and ribs for stability. It had three floors with stairs and walking panels. Then, louvered acoustic panels were installed. Because of the lack of light in the tunnel, reflective signs were put on for safety. Next, the top ventilation fans were installed. Finally, the NWBT was dragged into the tunnel by the loader to a stable position and fixed at the bottom.

3.4. Measurement Arrangement.

Figure 6 depicts the arrangement of the measuring points. The Point A and Point B were at the front and rear of the NWBT, respectively. The height of the measuring points from the ground was 1.2 m. The sampling frequency of the AOp sensor was 8 kHz. According to the research from Tian [20] and Uystepruyst
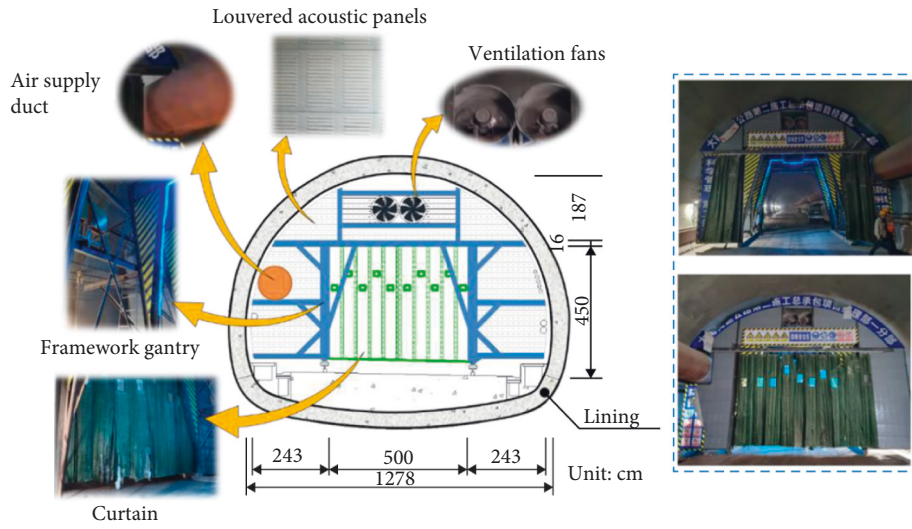
FIGURE 4: Description of NWBT.

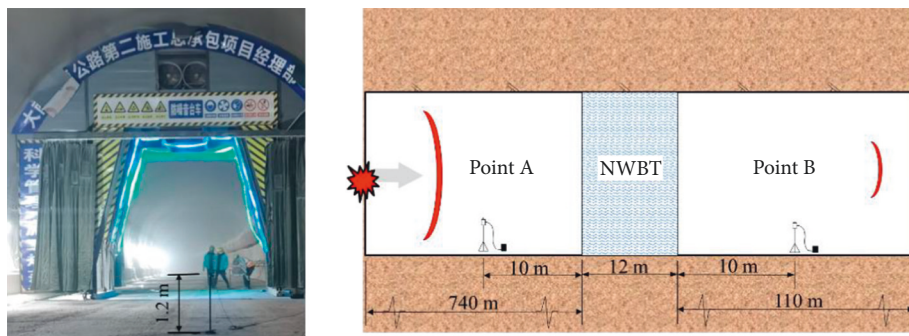FIGURE 5: Installation of NWBT.

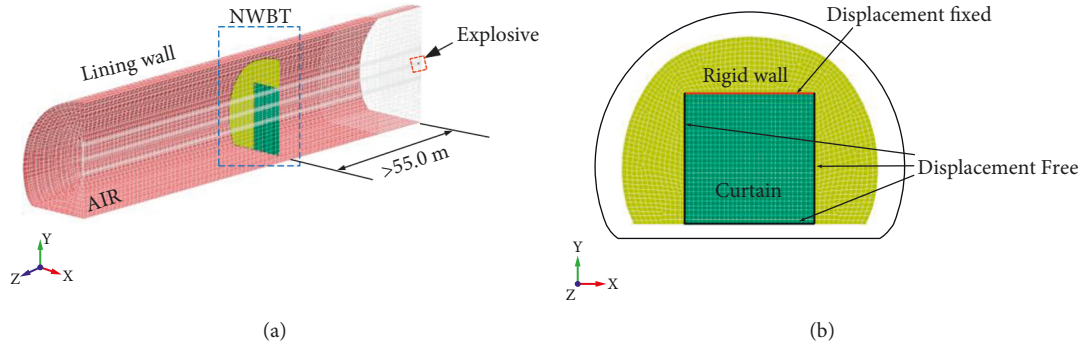FIGURE 6: Arrangement of the measuring points.

FIGURE 7: Numerical model: (a) profile graph and (b) symmetric grid of NWBT about YZ.

[21], after the blast, wave propagation distance exceeds 5 times the tunnel diameter, the wavefront has been gradually transformed into a plane wave with a certain thickness, and the pressure on the wavefront is basically uniform. The measurement points were set at the area of plane wave propagation, which in the experiments is longer than 55.0 m, and could exclude the interference of blast wave shape. Meanwhile, the working NWBT was placed at 110 m from the tunnel portal in order to facilitate the organization of tunnel construction.

4. Numerical Simulation

4.1. Overview of the Numerical Model. Since the measured pressure profiles cannot demonstrate the change process of the blast wavefront, a finite element method (LS-DYNA) was used, and the numerical model is shown in Figure 7. To simplify the model, the NWBT consisted of a rigid wall and a curtain, which were simplified as a single layer of the shell-mesh. The upper edge of the curtain was fixed to the rigid wall, and the lower end was free. The tunnel section area was 98 m^2. Air was the medium for the propagation of the blast waves. The lining wall whose material is shell-mesh confined the blast wave propagation. Because of the symmetry of the configuration, only one half of the airwave propagation domain was established. The symmetry of the model was established using a displacement constraint boundary, and the exit at both ends was a nonreflection boundary.

4.2. Material Models. The keywords ∗MAT_HIGH_EXPLOSIVE_BURN and ∗MAT_NULL were used to define the material properties of the explosion and air. The AOp caused by an explosion obeys the Jones–Wilkins–Lee law, which is expressed as follows:

$$P = A\left(1 - \frac{w}{VR_1}\right)\exp\left(\frac{-R_1}{V}\right) + B\left(\frac{w}{VR_2}\right)\exp\left(\frac{-R_2}{V}\right) + \frac{wE_0}{V}, \tag{3}$$

where A, B, R_1, R_2, and w are constants obtained from the test, E_0 is the initial internal energy ratio, and V is the relative volume, which was taken as 1.0. Table 1 provides these parameters.

The keyword ∗MAT_PLASTIC_KINEMATIC is suited to model isotropic, so it was used to define the lining concrete and rigid wall, which included the density ρ, modulus of elasticity E, Poisson's ratio μ, and yield stress σ, as shown in Table 2.

Meanwhile, the material (∗MAT_PLASTIC_KINEMATIC) is also suited to kinematic hardening plasticity, which is commonly used to simulate the aircraft windshield structure in bird striking analysis [17], bulletproof vest material [18], and protective mesh for rockfall [19]. The same applies to simulating maize plants [22], human ankle structure [23], and other flexible materials. So, the No. 3 material model in the Hyper-mesh Material Library (∗MAT_PLASTIC_KINEMATIC) was selected as the simulation material of NWBT curtain by comparing with information of the Hyper-mesh Material Library database as shown in Table 2. The curtain material parameters were taken with reference to these analyses.

4.3. Validation of Model. Measurements of the blast wave in the unobstructed tunnel were tested several times, and the comparison of the measurements values with the numerical simulations is shown in Figure 8. The horizontal coordinates in the figure are the logarithms of the scaled distances, and the vertical coordinates are the logarithms of the AOp. From the figure, the decay laws of the field measurements and numerical simulations are similar; and the slope of the curve is relatively close. Therefore, it can be considered that the numerical model is appropriate to the on-site practice conditions.

5. Results and Discussion

5.1. Determination of Critical Waveform Pulse. Figure 9 shows the measurement of the pressure profiles. The difference between P^* at Point A and Point B was very slight because there was no NWBT installed at this time. There were multiple pulses in the waveform curve, which was due to the multiple blast sources induced by millisecond delayed blasting and was also related to the reflected waves caused by the walls in the tunnel. The Friedlander waveform equation describes a single pulse, so the priority should be to select the

TABLE 1: Parameters used for the Jones–Wilkins–Lee law describing the explosive material.

Initial energy of explosives, E_0 (kJ/kg)	Density, ρ (kg/m^3)	A ($\times$ 1011 Pa)	B ($\times$ 109 Pa)	R_1	R_2	w
2.0×109	1600	2.29	5.5	6.5	1.0	0.35

TABLE 2: Structural material parameters used.

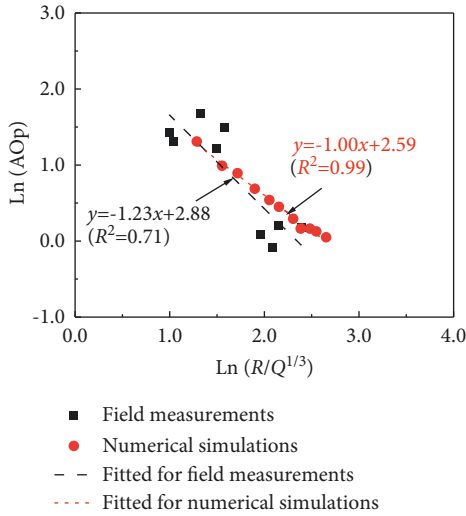| Type	Density, ρ (kg/m^3)	Modulus of elasticity, E (GPa)	Poisson's ratio, μ	Yield stress, σ (MPa)
Lining concrete	2400	32.5	0.20	30.0
Rigid wall	1200	8.0	0.33	10.0
Curtain	400	0.009	0.33	—

FIGURE 8: Comparison of measured with numerical simulations.
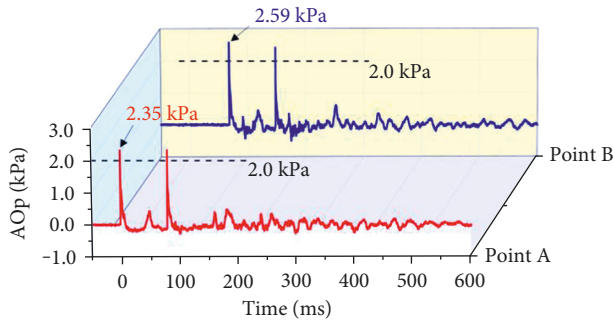

FIGURE 9: Pressure profiles of point A and point B.

most representative pulse waveform through a suitable method.

Wavelet analysis is considered to be an effective method for analyzing signals in the time domain [24, 25]. The wavelet analysis results of the pressure files are shown in Figure 9. The db8 wavelet function was used, and at the time-energy distribution of the AOp, four energy peaks were observed at Point A and Point B. The first and second pulses had larger energies than other pulses and almost the same time difference (68 ms) in the time domain, and the third and fourth pulses may have been caused by eddy currents or reflected waves. For the sake of comparison, the first pulse

was chosen as the descriptive curve of the Friedlander waveform.

5.2. Characteristics of Blast Wave. The first pulse in Figure 9 is chosen as the blast waveform for comparison. The Friedlander equation described the pressure pulse of the blast wave very well, as shown in Figure 10. Compared with the peak pressure in explosion work [10], the peak pressure P^* of the explosion wave during the tunnel fracturing work was significantly smaller and the duration t_d was shorter. The positive pressure region had a shorter duration than the negative pressure region.

The characteristic parameters of the blast wave from Point A and Point B are shown in Figures 10 and 11, and the fitted equations are as follows:

$$P(t) = 2.35\left(1 - \frac{t - 0.125}{8.5}\right)e^{-3.38t - 0.125/8.5}, \left(R^2 = 0.79\right), \quad (4)$$

$$P(t) = 2.59\left(1 - \frac{t - 68.125}{7.8}\right)e^{-3.39t - 68.125/7.8}, \left(R^2 = 0.88\right). \quad (5)$$

The calculated impulse I^*_{fitted} was consistent with the actual I^*. The Friedlander equation for Point A is shown in (4), with a decay coefficient b of 3.38 and a correlation coefficient R^2 of 0.79. The Friedlander equation for measurement Point B is shown in (5), with a decay coefficient b of 3.39 and a correlation coefficient R^2 of 0.88. The decay coefficient b was close to that obtained for a free-air incident blast wave [10].

5.3. Resistance Effect of the NWBT. The threshold of the AOp is 2.0 kPa in the Chinese code Blasting Safety Regulations (GB6722-2014), which is the safe pressure considering human health. When the NWBT is not operating, the AOp inside the tunnel is beyond the threshold pressure (as shown in Figure 9). The AOp was effectively attenuated to meet the requirements of the code when the NWBT was operating, as shown in Figure 12. The first pressure peak in the energy curve of Point B in Figure 13 is decomposed into several peaks in Figure 14(b), with smaller energy values, and the AOp was effectively weakened.

The changes of the blast wave parameters with operating NWBT are shown in Figure 15 and Table 3. First, the
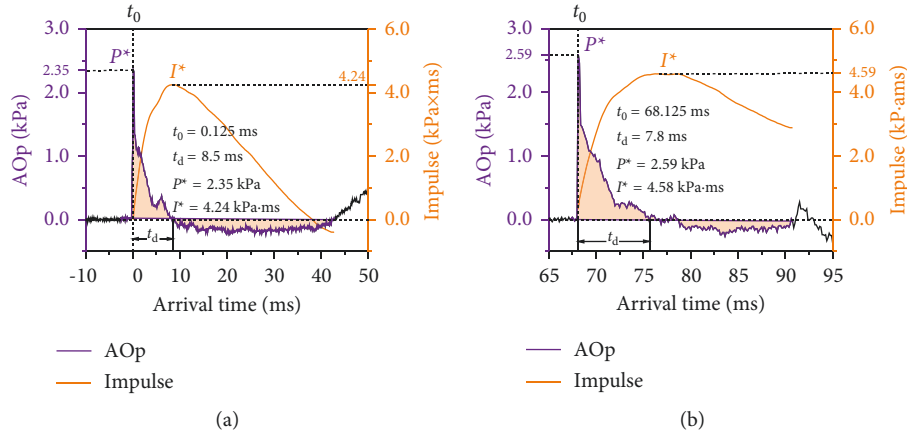
FIGURE 10: Time profiles of AOp and impulse: (a) Point A and (b) Point B.
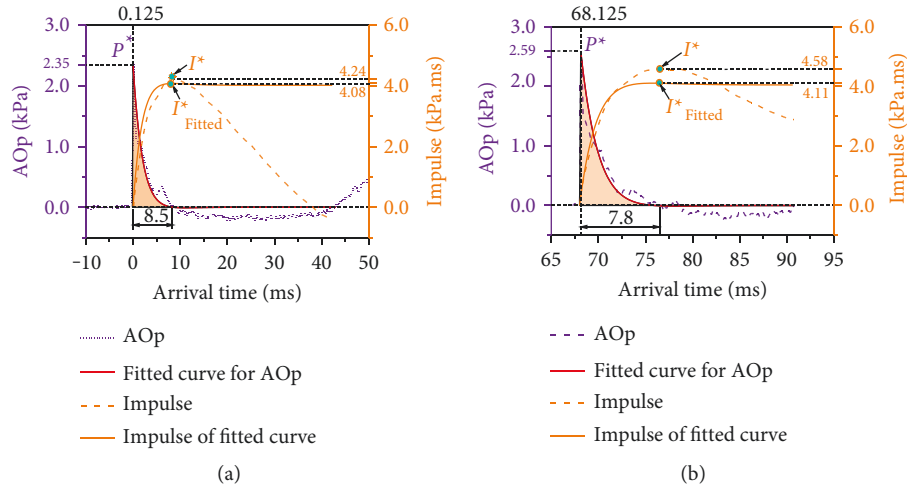

FIGURE 11: Friedlander equation fitting of the AOp curve: (a) Point A and (b) Point B.
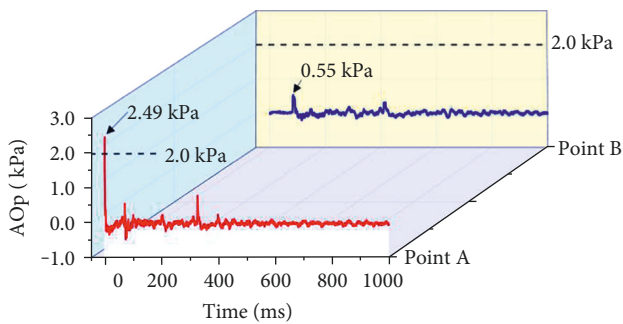

FIGURE 12: AOp time histories with working NWBT.

comparison of pressure profiles between the measured and numerical simulation shows that the numerical model with NWBT is still reliable. When the NWBT is operating with a closed wave-blocking curtain, the peak pressure P^* was effectively weakened from 2.49 kPa to 0.55 kPa, a decrease of 79.3%. The energy density decreased from 0.33 kJ to 0.016 kJ, a decrease of more than 90%. The AOp of the explosion was effectively reduced by the NWBT.

Similarly, the time-energy curve showed that the first pulse of the blast wave was also the most typical pressure wave when the NWBT was operating. By analyzing the blast parameters of the first pulse of the blast wave, the NWBT operation caused a significant change in the peak pressure P^* and time duration td at the front and rear measurement points of the device. However, there was no significant change in the impulse I^*. The NWBT reduced the blast wave pressure P^*, but the impulse I^* did not decrease significantly due to the extended duration td of the blast wave.

5.4. Changes in Blast Wavefront by NWBT. The flow field near the NWBT was studied using numerical simulations. Figure 16 shows that the AOp curve in the simulation was consistent with the measured field. When a blast wave moved in the tunnel, the pressure attenuation was limited due to the partial confinement. When the blast wave bypassed the NWBT, it was absorbed, reflected, or diffracted. Figure 17 shows the digital camera images of the swaying process of the curtain when it was impacted by the blast wave, and this process was reproduced by the numerical
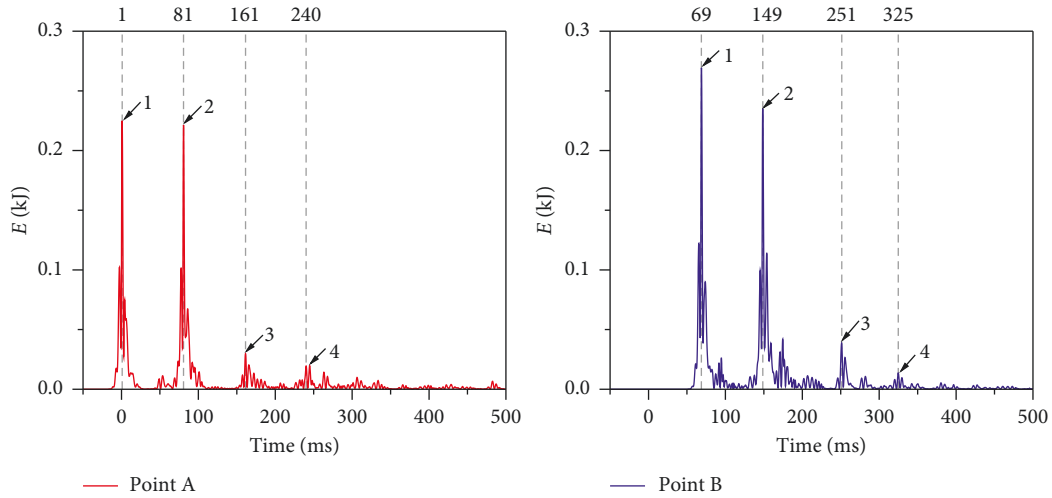
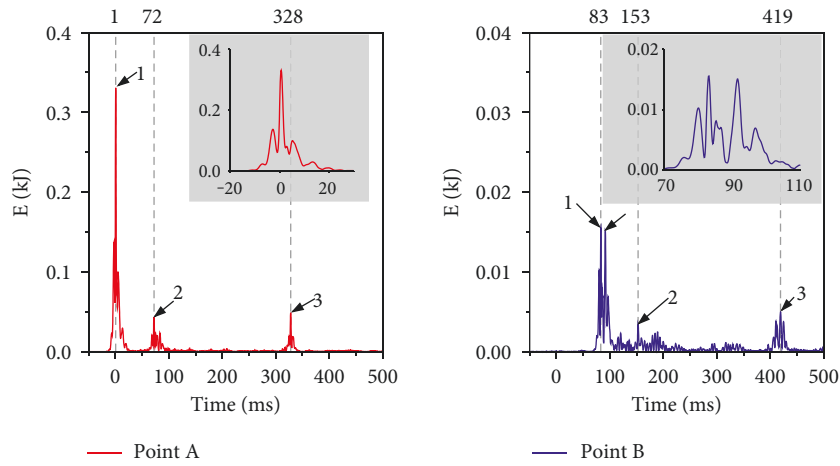Figure 13: Time-energy distributions of AOp.

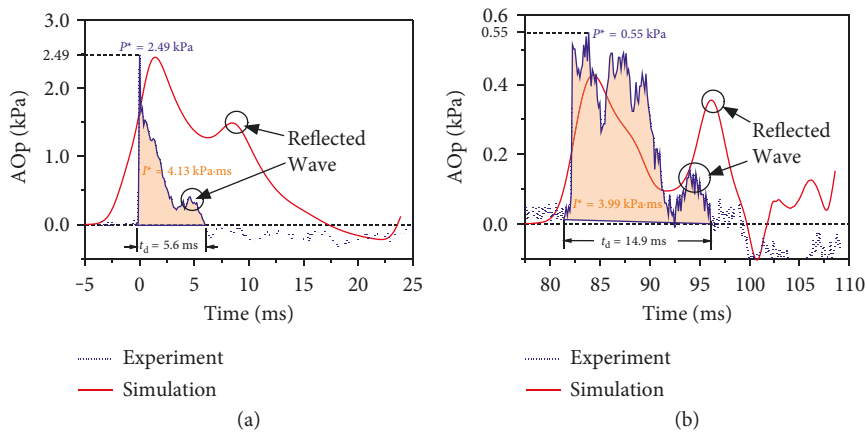Figure 14: Time-energy distribution of AOp with working NWBT.

Figure 15: Time profiles of AOp and impulse: (a) Point A and (b) Point B.

Table 3: Comparison of blast parameters at point A and point B.

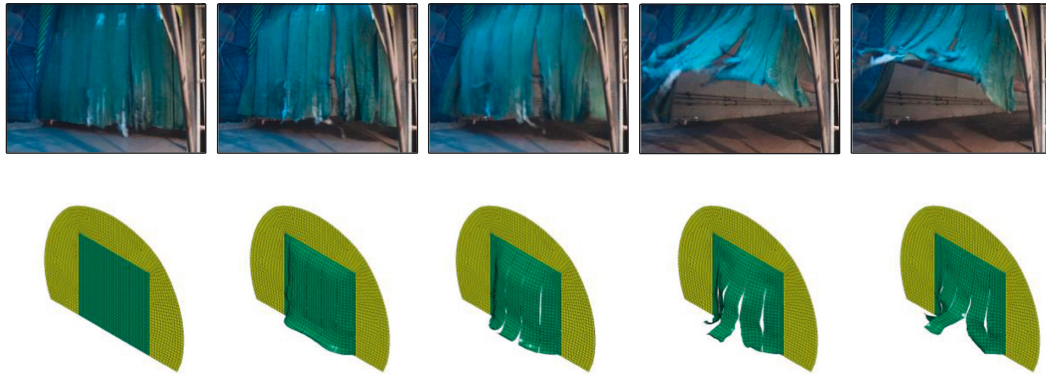| Measurement point	Peak pressure, P^* (kPa)	Time duration, t_d (ms)	Impulse, I^* (kPa·ms)	Energy, E (kJ)
Point A	2.49	5.6	4.13	0.33
Point B	0.55	14.9	3.99	0.016

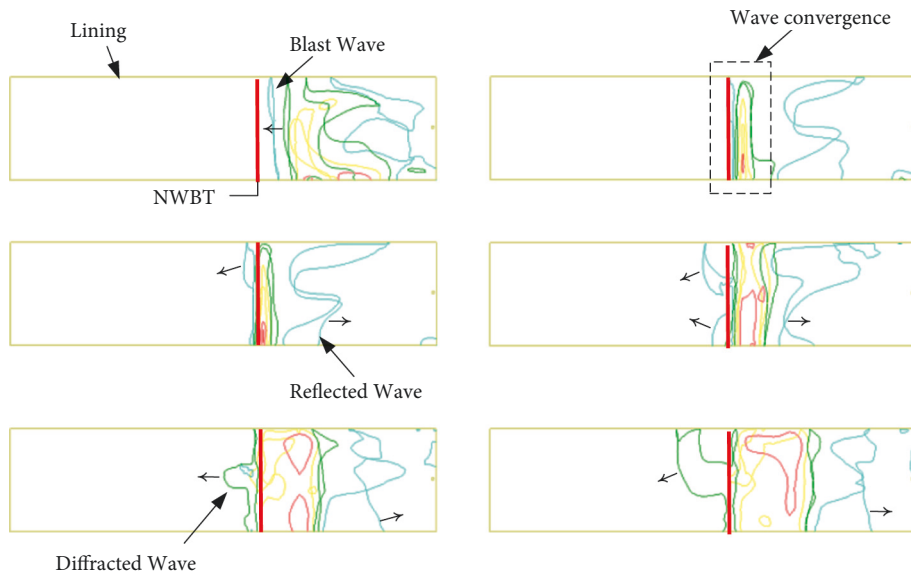FIGURE 16: Processes of rigid wall and curtain during blast wave impact.

FIGURE 17: Blast wavefront near rigid wall and wave-blocking curtain.
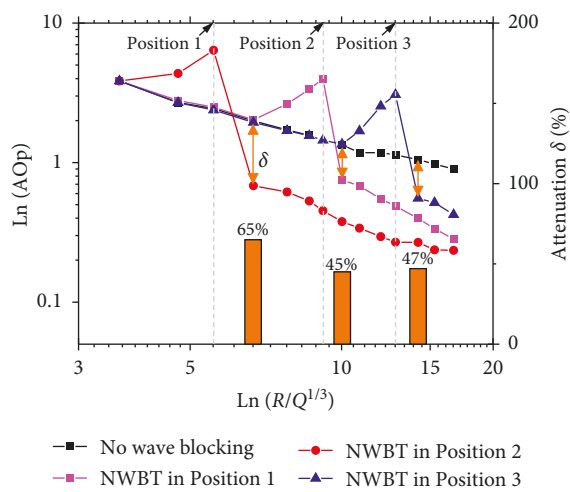

FIGURE 18: Blast wavefront near rigid wall and wave-blocking curtain.

simulations. The rigid wall blocked and attenuated most of the pressure waves, while the rotation of the curtain corresponded to energy conversion of the blast wave. The kinetic energy of the blast wave was transformed into the rotational energy of the curtain and the elastic potential energy of the curtain.

The configuration of the blast wave was greatly compressed due to the reflection and diffraction of the rigid wall and curtain. The blast wave was significantly compressed, and the pressure of the blast wave significantly increased due to the NWBT block. The diffracted blast waves bypassing the rigid wall reached the backside and converged again, thus continuing to propagate in the tunnel. The reflected wave shown by the curve in Figure 15(a) is formed by the reflection of the blast wave after impacting the rigid wall. The reflected wave shown by the curve in Figure 15(b) is formed due to the bypassing of the diffracted blast waves.

5.5. *Optimal Working Area of NWBT.* In order to optimize the wave-blocking effect, the NWBT was placed at different locations to compare the degree of pressure attenuation, as shown in Figure 18. Taking the measurement point after NWBT as a comparison, the degree of pressure attenuation is greater as soon as possible at a shorter distance during the blast wave propagation. While the pressure decay at locations 2 and 3 is close, the pressure in the intercepted area is less when the

NWBT is placed closer to the blast source. Therefore, although the NWBT needs to be installed after the secondary lining trolley, a shorter distance from the blast source to NWBT available will better perform its wave-blocking effect.

6. Conclusion and Discussion

Compared with the bamboo shields and bulky wave barriers currently used in the construction, the NWBT achieves great wave-blocking without interrupting traffic in the tunnel. Compared with spoilers, NWBT achieves a larger wave-blocking area and can completely block blast waves. The materials used in NWBT are easy to obtain and the assembly process is simple for engineers, making it very easy to use. The conclusions obtained from the field measurements and numerical analysis in this study are as follows:

(1) The waveforms of tunnel blasting is significantly different from the blast waveform of a single explosive, the pressure profile has the property of being multipeaked. When the first pressure pulse was selected as the critical pressure waveform, the waveform was well fitted by the Friedlander equation. The peak pressure P^* and impulse I^* of the blast wave were obtained. The values of the attenuation coefficient b of the Friedlander equation for the blast waves at two measurement points inside the tunnel were 3.38 and 3.39, respectively. In the absence of any control measures and device work, the peak AOp of the blast wave exceeded the threshold pressure of 2.0 kPa of the Chinese regulations.

(2) The NWBT played a very effective role in reducing the blast wave pressure. The peak pressure P^* was effectively weakened from 2.49 kPa to 0.55 kPa, a decrease of 79.3%, which meets the pressure safety requirement. The duration td of the blast wave increased from 5.6 to 14.9 ms, and the impulse I^* did not decrease due to the increase in the duration t_d.

(3) The interaction process between the blast wave and the NWBT contains a complex flow field. Results from numerical simulations visually indicated that absorption, reflection, or diffraction of the blast wave occurred near the NWBT. The reflected waves in the measured pressure profiles were caused by the diffraction of the blast wave bypassing the block of the NWBT.

(4) The degree of attenuation of blast waves is different for varying placements of NWBT in the tunnel. A shorter distance from the NWBT to the source of the explosion, the more it can play its role in blocking the wave.

The NWBT presented in this study has many advantages over other wave-blocking devices such as spoilers and blast doors. The advantages such as high wave elimination efficiency, simple structure, low cost, and convenient installation make it suitable for traffic tunnelling constructions. Of course, the application of the structure needs more practical engineering to verify.

Data Availability

The data used to support the findings of this study are available from the corresponding author upon request.

Conflicts of Interest

The authors declare that they have no conflicts of interest.

Acknowledgments

References

[1] H. Kang, X. Fang, Y. Zou, Q. Tian, and Y. Fang, "Propagation law of blasting-caused shock-wave in tunnel," *Tunnel Construction*, vol. 41, pp. 130–137, 2021.

[2] F. Faramarzi, M. A. Ebrahimi Farsangi, and H. Mansouri, "Simultaneous investigation of blast induced ground vibration and airblast effects on safety level of structures and human in surface blasting," *International Journal of Mining Science and Technology*, vol. 24, no. 5, pp. 663–669, 2014.

[3] P. P and K. Tachom, "Monitoring and control airblast overpressures in an open pit coal mine," *Physics and Chemistry of the Earth, Parts A/B/C*, vol. 121, Article ID 102960, 2021.

[4] C. W. Lee, J. Kim, and G. C. Kang, "Full-scale tests for assessing blasting-induced vibration and noise," *Shock and Vibration*, vol. 2018, pp. 1–14, 2018.

[5] Y. Fang, Y. L. Zou, J. Zhou, Z Yao, S. Lei, and W. Yang, "Field tests on the attenuation characteristics of the blast air waves in a long road tunnel: a case study," *Shock and Vibration*, vol. 2019, pp. 1–11, 2019.

[6] R. Rodríguez, C. Lombardía, and S. Torno, "Prediction of the air wave due to blasting inside tunnels: approximation to a phonometric curve," *Tunnelling and Underground Space Technology*, vol. 25, no. 4, pp. 483–489, 2010.

[7] R. Rodríguez, J. Toraño, and M. Menéndez, "Prediction of the airblast wave effects near a tunnel advanced by drilling and blasting," *Tunnelling and Underground Space Technology*, vol. 22, no. 3, pp. 241–251, 2007.

[8] P. Prochazka and D. Jandeková, "Effect of explosion source location on tunnel damage," *International Journal of Protective Structures*, vol. 11, no. 4, pp. 448–467, 2020.

[9] N. Chandra, S. Ganpule, N. N. Kleinschmit et al., "Evolution of blast wave profiles in simulated air blasts: experiment and computational modeling," *Shock Waves*, vol. 22, no. 5, pp. 403–415, 2012.

[10] V. Karlos, G. Solomos, and M. Larcher, "Analysis of the blast wave decay coefficient using the Kingery-Bulmash data," *International journal of protective structures*, vol. 7, no. 3, pp. 409–429, 2016.

[11] A. M. Benselama, M. J. P. William-Louis, F. Monnoyer, and C. Proust, "A numerical study of the evolution of the blast wave shape in tunnels," *Journal of Hazardous Materials*, vol. 181, no. 1-3, pp. 609–616, 2010.

[12] D. Zou, "Study and discussion of air overpressure produced by blasting near high residential buildings," *Engineering Blasting*, vol. 12, pp. 79–83, 2006.

[13] K. Wang, H. Hao, S. Jiang, W. Cai, Y. Zhang, and Z. Wang, "Experimental study on the characteristics of overpressure wave to ventilation facilities during gas explosion and automatic shock relief devices," *Geomatics, Natural Hazards and Risk*, vol. 11, no. 1, pp. 2361–2384, 2020.

[14] Q. F. Zhang, *Research on Attenuation Law of Shock Wave in Tunnel Blasting and Design of Reducing Equipment*, (Master's Thesis in Chinese), Shandong University of Science and Technology), Qingdan, Shandong, 2019.

[15] B. Zhao, J. Zhao, C. Cui et al., "Simulation analysis of influence of spoiler structural parameters on shock wave attenuation characteristics," *Chinese Journal of High Pressure Physics*, vol. 32, no. 02, pp. 158–166, 2018.

[16] S. Sha, Z. Chen, and X. Jiang, "Influences of obstacle geometries on shock wave attenuation," *Shock Waves*, vol. 24, no. 6, pp. 573–582, 2014.

[17] P. Yu, S. Yu, S. He, X. Huang, and W. Yun, "Inversion for constitutive model parameters of bird in case of bird striking," *Shock and Vibration*, vol. 2022, pp. 1–10, 2022.

[18] J. Dominiak and Z. Stempień, "Finite-element-based modeling of ballistic impact on a human torso protected by textile body armor," *Innovative Materials & Technologies in Made-Up Textile Articles, Protective Clothing and Footwear*, 2012.

[19] S. He, S. Yan, Y. Deng, and W. Liu, "Impact protection of bridge piers against rockfall," *Bulletin of Engineering Geology and the Environment*, vol. 78, no. 4, pp. 2671–2680, 2019.

[20] Z. M. Tian, Y. B. Wu, and Q. F. Luo, "Characteristics of in-tunnel explosion-induced air shock wave and distribution law of reflected shock wave load," *Journal of Vibration and Shock*, vol. 30, no. 1, p. 6, 2011.

[21] D. Uystepruyst and F. Monnoyer, "A numerical study of the evolution of the blast wave shape in rectangular tunnels," *Journal of Loss Prevention in the Process Industries*, vol. 34, pp. 225–231, 2015.

[22] J. Qin, Y. Yin, Z. Liu et al., "Optimisation of maize picking mechanism by simulation analysis and high-speed video experiments," *Biosystems Engineering*, vol. 189, pp. 84–98, 2020.

[23] L. F. Gabler, M. B. Panzer, and R. S. Salzar, "High-rate mechanical properties of human heel pad for simulation of a blast loading condition," in *Proceedings of the IRCOBI Conference*, pp. 796–808, Berlin: Germany, 2014, September.

[24] X. M. Zhang, X. S. Zhou, L. C. Wang et al., "Attenuation of blast wave in a large-section tunnel," *Explosion and Shock Waves*, vol. 40, pp. 119–129, 2020.

[25] T. Ling, "Laws of energy distribution in different frequency bands for blast vibration signals," *Journal of Central South University of Technology*, vol. 35, pp. 310–315, 2004.